Aging and central vision loss: Relationship between the cortical macro-structure and micro-structure

Anton L. Beer [*], Tina Plank, Mark W. Greenlee

Institut für Psychologie, Universität Regensburg, Regensburg, Germany

ARTICLE INFO

ABSTRACT

Aging and central vision loss are associated with cortical atrophies, but little is known about the relationship between cortical thinning and the underlying cellular structure. We compared the macro- and micro-structure of the cortical gray and superficial white matter of 38 patients with juvenile (JMD) or age-related (AMD) macular degeneration and 38 healthy humans (19–84 years) by multimodal MRI including diffusion-tensor imaging (DTI). A factor analysis showed that cortical thickness, tissue-dependent measures, and DTI-based measures were sensitive to distinct components of brain structure. Age-related cortical thinning and increased diffusion were observed across most of the cortex, but increased T1-weighted intensities (frontal), reduced T2-weighted intensities (occipital), and reduced anisotropy (medial) were limited to confined cortical regions. Vision loss was associated with cortical thinning and enhanced diffusion in the gray matter (less in the white matter) of the occipital central visual field representation. Moreover, AMD (but not JMD) patients showed enhanced diffusion in lateral occipito-temporal cortex and cortical thinning in the posterior cingulum. These findings demonstrate that changes in brain structure are best quantified by multimodal imaging. They further suggest that age-related brain atrophies (cortical thinning) reflect diverse micro-structural etiologies. Moreover, juvenile and age-related macular degeneration are associated with distinct patterns of micro-structural alterations.

1. Introduction

During the life-span even healthy people experience a change in cognitive functions (Grady, 2012). These changes are likely mediated by the cellular architecture of the cortical white (WM) and gray (GM) matter. Post-mortem studies in humans and animal research showed that normal aging may be associated with neural loss (Pakkenberg et al., 2003), reduced dendritic branching (de Brabander et al., 1998) and synaptic density (Peters et al., 2008), myelin degeneration (Pakkenberg et al., 2003), alterations of other glial structures (Brown, 2009; Nichols et al., 1993; Peters, 2009), or excessive iron depositions (Zecca et al., 2004). In-vivo human brain imaging studies showed that normal aging is associated with atrophies of the brain macro-structure such as reduced gray (Salat et al., 2004) and white matter (Tang et al., 1997) volume, thinner gray matter (Lemaitre et al., 2012; Salat et al., 2004), and decreased gray matter volume and density (Sowell et al., 2003; Walhovd et al., 2005).

The brain morphology is also affected by sensory deprivation such as central vision loss (CVL). Central vision loss most often results from macular dystrophies or degeneration due to cellular damage of the fovea or adjacent retina. Macular degeneration may reflect an age-related disease (AMD) (Resnikoff et al., 2004) caused by the accumulation of drusen that impairs the metabolism of retinal cells (Holz et al., 2004). Alternatively, juvenile macular dystrophies (JMD) may result from hereditary eye diseases such as Stargardt's disease, cone-rod dystrophies, and central areolar choroidal dystrophies (Boon et al., 2009). The retinal damage in AMD and JMD patients is accompanied by atrophies of cortical structures that represent the deprived visual field - known as 'lesion projection zone' (LPZ). Reductions of the cortical gray matter volume (Hernowo et al., 2014; Plank et al., 2011) and density (Boucard et al., 2009) as well as cortical thinning (Prins et al., 2016) were observed in the lesion projection zone of the primary (V1) and secondary (V2) visual cortex of CVL patients. Possibly, this atrophy reflects secondary degeneration due to the lack of visual input.

The cortical thinning associated with aging and central vision loss likely reflects structural alterations at a cellular level. However, the relationship between the brain macro-structure and the underlying micro-structure still remained unclear. This gap may be bridged by diffusion-weighted imaging, a non-invasive magnetic resonance imaging (MRI) technique that is sensitive to the diffusion of water and, hence, to the cellular structure of the brain (Beaulieu, 2002). A major model in

Abbreviations

AD	axial (longitudinal) diffusion
AMD	age-related macular degeneration
CSF	cerebro-spinal fluid
CT	cortical thickness
CVL	central vision loss
DTI	diffusion-tensor imaging
DWM	deep white matter
e1, e2, e3, e4	eccentricity representations of visual field from central to peripheral
FA	fractional anisotropy
GM	gray matter (cortical)
IVC	inter-voxel coherence
JMD	juvenile macular dystrophy
MD	mean diffusion

MO	mode of diffusion
MRI	magnetic resonance imaging
NV	normal vision (control group)
PCA	principal component analysis
PGB	pial-gray matter boundary
RD	radial (perpendicular) diffusion
ROI	region-of-interest
SWM	superficial white matter
T1w	T1-weighted MRI
T2w	T2-weighted MRI
V1	primary visual cortex
V2	secondary visual cortex
v1, v2, v3	first, second, and third eigenvector of the tensor model
WGB	white-gray matter boundary
WM	white matter
$\lambda_1, \lambda_2, \lambda_3$	first, second, and third eigenvalue of the tensor model

diffusion-weighted imaging is the tensor model (Basser et al., 1994). Diffusion-tensor imaging (DTI) describes the diffusion by an ellipsoid composed of three eigenvectors (v_1, v_2, v_3) and their corresponding eigenvalues (λ_1, λ_2, λ_3) (see Fig. 1b). Based on this model several measures of diffusion-strength such as axial (AD), radial (RD), and mean diffusion (MD) may be derived. In addition, it provides several measures for the shape of diffusion such as fractional anisotropy (FA) (Basser and Pierpaoli, 1996), the mode of diffusion (MO) (Ennis and Kindlmann, 2006), and inter-voxel coherence (IVC) (Pfefferbaum et al., 2000).

Although several previous studies examined DTI properties in humans as a function of aging or central vision loss, it remained difficult to draw direct conclusions about the relationship between the brain macro- and micro-structure. Previous studies focused on either a limited set of brain regions of interest (ROI) (e.g., Helenius et al., 2002; Pfefferbaum et al., 2000), major white matter fiber tracts (Malania et al., 2017; Ogawa et al., 2014; Penke et al., 2010; Sullivan et al., 2010; Zahr et al., 2009), or a white matter FA-skeleton (Burzynska et al., 2010; Damoiseaux et al., 2009). With the exception of a few volumetric voxel-based whole-brain approaches (Camara et al., 2007; Draganski et al., 2011), previous studies examined only the deep white matter (DWM). However, cortical atrophies are likely mediated by the micro-structure of the cortical gray matter (GM) and the region below the white-gray matter boundary (WGB) known as superficial white matter (SWM). The superficial white matter is characterized by a high proportion of local association fibers (also called 'U' fibers) (Oishi et al., 2008) and a high density of interstitial neurons (Suarez-Sola et al., 2009). Although the superficial white matter is affected by neurological (Phillips et al., 2016) and psychiatric (Eastwood and Harrison, 2003) disorders or during brain development (Wu et al., 2014), it is still unclear how it is affected by aging and sensory deprivation. Moreover, little is known about how macro-structural and micro-structural measures of cortical atrophies are related. Currently, only descriptive comparisons between DTI-based and tissue-based measures have been performed (Draganski et al., 2011).

Therefore, this study examined the brain macro- and micro-structure of 38 patients with central vision loss and 38 age-matched healthy humans in the age range from 19 to 84 years (Fig. 1a) by multimodal MRI including DTI. Cortical thickness, tissue-dependent measures (e.g., T1-weighted and T2-weighted intensities) as well as measures of diffusion-strength (e.g., MD) and diffusion-shape (e.g., FA) were compared. Inter-measure dependencies were evaluated by a factor analysis. A surface-based analysis was adopted that focused on the cortical gray and the superficial white matter. Effects of central vision loss were further quantified within cortical regions of interest.

2. Material and methods

2.1. Sample

Data were collected from 38 patients with binocular central vision loss (CVL) and 38 age-matched controls with normal vision (NV) (Fig. 1a). Twenty-five of the patients suffered from JMD, the remaining 13 patients from AMD with geographic atrophy. Among JMD patients, the central vision loss resulted from a cone-rod dystrophy (7), cone dystrophy (1), central areolar choroidal dystrophy (2), Stargardt's disease (14), or from an unclassified hereditary macular dystrophy (1) as diagnosed by ophthalmologists. The mean scotoma size as examined by Goldmann perimetry was 19.6° (diameter) of visual angle in the JMD group and 14.6° of visual angle in the AMD group (not significant). The mean disease duration was 16.0 years in the JMD group and 7.3 years in the AMD group [t(36) = 3.14; p = .003]. Moreover, the AMD group (0.15) had an overall better visual acuity (mean decimal visual acuity in the better eye) than the JMD group (0.09) [t(36) = −2.8; p = .009]. However, reading speed (mean words per minute) was lower in AMD patients (40.6) than in JMD patients (64.5) [t(35) = 2.1; p = .045]. Both patient groups reported similar constraints on their activities of daily living as assessed by an in-house questionnaire. Assessments followed procedures as previously described (Plank et al., 2011; Rosengarth et al., 2013). The mean age was 53.8 years (range 19–84) in the patient group (44.3 for JMD and 72.1 for AMD) and 52.5 years (range 23–83) in the control group. The patient group contained 23 men/15 women and the control group 19 men/19 women. A subset of the data was used in previous studies with a different research question (Beer et al., 2011; Hernowo et al., 2014; Plank et al., 2011, 2013, 2017; Prins et al., 2016; Rosengarth et al., 2013). All participants gave written informed consent prior to the study and received monetary compensation (20 Euro) for their participation. The procedure was approved by the ethical board of the University of Regensburg.

2.2. Data acquisition

All MRI data was acquired by a 3 T Allegra head scanner (Siemens AG, Erlangen, Germany) over a period of two years. For each participant one high-resolution T1-weighted structural and one diffusion-weighted measurement were acquired. The anatomical T1-weighted images (repetition time: 2250 ms, echo time: 2.6 ms, flip angle: 9°, voxel size: 1 x 1 × 1 mm³, field of view: 256 × 256 mm²) were acquired by a MPRAGE (magnetization prepared rapid acquisition gradient echo) sequence
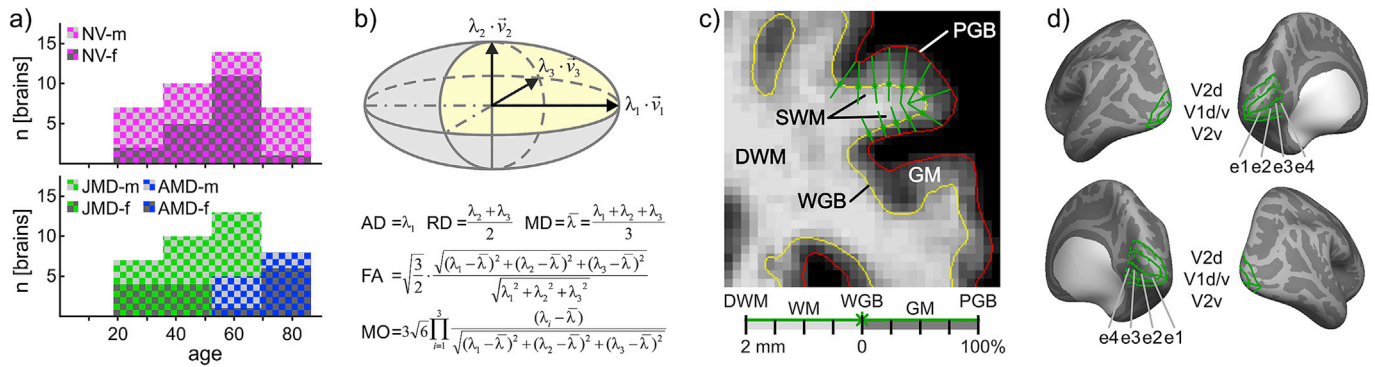
Fig. 1. Methods. a) Age histogram of the study sample, shown separately for women (NV-f) and men (NV-m) of the control group (top) with normal vision (NV) and patients with central vision loss due to juvenile (JMD-f, JMD-m) or age-related (AMD-f, AMD-m) macular degeneration. b) Geometric illustration of the diffusion tensor model and calculation of axial diffusion (AD), radial diffusion (RD), mean diffusion (MD), fractional anisotropy (FA), and mode of diffusion (MO) based on eigenvalues (λ_1, λ_2, λ_3). c) Projection levels along the superficial white matter (SWM) and gray matter (GM) relative to the white-gray matter boundary (WGB) ranging from deep white matter (DWM) to pial-gray matter boundary (PGB). d) Regions of interest (ROI). Borders of primary (V1) and secondary (V2) visual areas, dorsal and ventral parts, and four eccentricity levels (e1 to e4) were defined and overlaid (green) on the inflated average surface.

across 160 sagittal slices. DTI data was acquired by a single shot spin-echo echo-planar sequence with a b-value of 1000 s/mm^2. Due to a software update on the scanner during the acquisition period, two DTI sequences were used. Forty-six participants were examined with a DTI sequence probing 30 isotropically distributed orientations and 5 interspersed b-zero weighted volumes of 54 axial slices (repetition time: 7200 ms, echo time: 95 ms, flip angle: 90°, 2.5 x 2.5 × 2.5 mm^3, field of view: 240 × 240 mm^2). The remaining participants were examined by a DTI sequence probing 64 isotropically distributed orientations and 8 interspersed b-zero weighted volumes of 54 axial slices (repetition time: 5400 ms, echo time: 95 ms, flip angle: 90°, 2.5 x 2.5 × 2.5 mm^3, field of view: 240 × 240 mm^2). Although acquisition type was equally distributed across groups and previous research showed that DTI parameters are fairly stable at 30 or more diffusion orientations, acquisition sequence was added as nuisance regressor in the analyses.

2.3. Cortical reconstruction

T1-weighted structural images were automatically reconstructed by Freesurfer version 5.3 (Martinos Center for Biomedical Imaging, Charlestown, MA) (Fischl, 2012). The reconstruction followed procedures as previously described (Beer et al., 2009, 2011). In brief, T1-weighted images were intensity normalized (including non-uniform normalization) (Zheng et al., 2009) and automatically segmented into gray and white matter structures. Then, the boundary between white and gray matter (WGB) was automatically tessellated and corrected for topologic inaccuracies. Finally, the cortical surface was deformed, inflated, and registered to a spherical atlas preserving the individual folding patterns of sulci and gyri. Moreover, the reconstruction provides several macroscopic brain measures including cortical thickness, gray matter volume, cortical surface area, and cortical gyrification measures (Van Essen and Drury, 1997). These include the intrinsic curvature index reflecting spherical indentations of the surface (large values meaning more indentations) and the folding index reflecting elongated surface flutes (large values meaning more folding).

2.4. DTI processing

The DTI images were analyzed by the FMRIB's Diffusion Toolbox (FDT) version 2.0 of FSL (Centre for Functional Magnetic Resonance Imaging of the Brain, University of Oxford, Oxford, UK) (Woolrich et al., 2009). Pre-processing included correction for head motion and eddy current distortions to a reference volume (first b-zero) and correction of diffusion vectors. The reference volume was automatically registered

(linear rigid-body) to the T1-weighted images. Image registrations were manually inspected and corrected if necessary. Following pre-processing, the tensor model (Basser et al., 1994) (see Fig. 1b) was calculated for each voxel.

2.5. Structural brain measures

The brain macro- and micro-structure was quantified by several tissue-dependent and diffusion-based measures. Diffusion-based measures (Fig. 1b) consisted of the three eigenvalues (λ_1, λ_2, λ_3) of the tensor model (Basser et al., 1994) and several derived measures. This included measures of diffusion-strength: mean (MD), axial (longitudinal) (AD), and radial (perpendicular) diffusion (RD). Note that AD corresponds to the major eigenvalue (λ_1). In addition, measures of diffusion-shape such as fractional anisotropy (FA), the mode of diffusion (MO), and the inter-voxel coherence (IVC) were calculated. FA is a normalized measure of anisotropy ranging from 0 (isotropic) to 1 (anisotropic diffusion) (Basser and Pierpaoli, 1996). MO describes the mode of anisotropic diffusion along a normalized continuum from −1 (planar) to +1 (tubular) (Ennis and Kindlmann, 2006). IVC reflects the average difference angle of the primary eigenvector between a voxel and its adjacent voxels (weighted by FA and distance) (Pfefferbaum et al., 2000). The mean angle was rescaled to a maximum of 1 and subtracted from 1 resulting in values ranging from 0 (incoherence: different orientation across voxels) to 1 (coherence: same orientation across voxels).

Tissue-dependent measures included T1-weighted (T1w) and T2-weighted (T2w) intensities. T1w were based on the MPRAGE images. T2w were based on the mean b-zero images of the DTI runs, which is essentially a T2-weighted signal. Both T1w and T2w values were normalized (rescaled) by the mean intensity of the white matter.

Finally, several measures of the brain macro-structure based on the Freesurfer reconstruction were examined. This included thickness estimates across the cortical surface but also global measures (brain volume, surface area, and gyrification indices). Two brains showed extreme values in gyrification indices (>3 standard deviations from the mean) and were excluded from this analysis.

2.6. Whole-brain analysis

All measures (except for global measures) were probed along nine projection levels relative to the white-gray matter boundary (WGB) of each individual reconstructed brain. This was done in order to evaluate differences (or similarities) between the gray and the superficial white matter and layer-specific properties within each structure. Projection

levels ranged from the deep white matter (DWM) 2 mm below the white matter surface to the white-gray matter boundary in steps of 0.5 mm and from the white-gray matter boundary to the pial-gray matter boundary (PGB) in steps of 25% of the cortical thickness. In order to assess the consequences of partial volume effects (e.g., values at gray matter voxels being contaminated by adjacent cerebro-spinal fluid), two projection levels (25% and 50%) beyond the pial-gray matter boundary were also analyzed.

All individual surface maps were spherically registered and mapped to the standard brain of Freesurfer. No volumetric smoothing was applied. Surface smoothing was performed by iterative nearest-neighbor averaging resulting in the equivalent of a 2D Gaussian kernel with a full-width half-maximum of 15 mm (Hagler et al., 2006). Note that this smoothing width is substantially less than in previous studies (22 mm diameter) examining age-related cortical thinning (Salat et al., 2004) as we wanted to avoid substantial blurring of the spatially limited effects expected by sensory deprivation.

For each measure and vertex, age-related and CVL-related variations across brains were assessed by a general linear model. The design matrix included regressors for age and CVL group, nuisance regressors for sex and MR sequence, and a constant. The age regressor coded the age for the whole sample relative to a reference age of 20 years. CVL-related variations were modeled by two regressors: JMD (1 for JMD patients, 0 otherwise) and AMD (1 for AMD patients, 0 otherwise). Note that these regressors model deviations from NV cases. Sex was coded by 1 for men (0 otherwise) and MRI sequence was coded by 1 for 30 orientations (0 otherwise). Subsequently, contrasts were defined: These included a Base effect (based on the constant regressor and corresponding to a NV brain at 20 years), an Age effect (slope of linear variations accounted by the age regressor), and a CVL group effect (combined contribution of the JMD and AMD regressor). Moreover, for a more detailed analysis of differences between JMD and AMD patients, separate contrasts were defined for the JMD and the AMD group effect.

The whole-brain analysis included three main steps: The first step of the analysis aimed to quantify global aspects of brain structure. Therefore, the mean values of the whole cortical surface (sparing the medial wall adjacent to subcortical structures) were compared for each of the three main contrasts. Second, a factor analysis based on principal components (PCA) (Jolliffe, 2002) was conducted to identify relevant and independent measures of brain structure. Third, cortical surface distributions of relevant measures were compared.

The PCA aimed to investigate redundancy and independence, respectively, across measures. Many previous studies restricted their analysis to one or a few primary measures (e.g., FA) or brain regions (e.g., WM). However, this approach may disregard unknown but potentially relevant markers of brain integrity. Hence, we adopted instead the data-driven approach of a factor analysis that clarifies which measures and projection levels are sensitive to the same or different cellular structures. Three analyses with the three main contrasts (Base level, Age effect, CVL effect) were conducted. The analysis was performed with custom-made Matlab (Mathworks) scripts. The data matrix containing the MRI measures and projection levels as variables and the vertices across the surface as observations was normalized (z-scaled). The number of principal components was identified by the Kaiser-Guttman criterion (eigenvalues greater than one). Subsequently, a varimax rotation of the reduced factor space was performed. Individual variables were assigned to one of the factors based on a minimum factor loading (correlation between variable and component) of 0.4 (Stevens, 2002) and the Fürntratt criterion (ratio of squared factor loading to communality $\geq$ 0.5) (Fürntratt, 1969).

Finally, a whole surface analysis was conducted for combinations of the variables (e.g., mean across projections) that were grouped together by the PCA. Surface-based significance maps were thresholded to a p-value of .01. Cluster-wise correction for multiple comparisons was performed by comparing voxel-wise significance maps (voxel-wise threshold of $p \leq .01$) with cluster-wise significance maps (cluster-wise threshold of $p \leq .01$) that were based on the Monte Carlo simulated distribution of

cluster size (CSD) as implemented in Freesurfer. Only clusters exceeding the CSD-simulated cluster size were preserved. As structural changes related to sensory deprivation were primarily expected in the occipital cortex, a less rigid cluster-wise correction (minimum cluster size of 50 mm^2) was adopted for the group effect (CVL vs. NV).

2.7. ROI analysis

For a more detailed quantification of the brain structure in CVL patients, a region-of-interest analysis of the visual cortex was performed (Fig. 1d). This was motivated by previous studies showing changes in brain structure (Boucard et al., 2009; Burge et al., 2016; Hernowo et al., 2014; Plank et al., 2011; Prins et al., 2016) and functional activity (Masuda et al., 2008) limited to visual cortex areas that represent the scotoma in the (central) visual field (lesion projection zone). Accordingly, ROIs of the primary (V1) and secondary (V2) visual cortex were defined by a surface-based atlas that mapped visual areas and eccentricity representations by population receptive fields (Benson et al., 2014). Both V1 and V2 were further sub-divided into four eccentricity representations of the visual field that covered similarly large cortical areas: e1 ($<$4.0° radius in visual angle), e2 (4.0°–8.5°), e3 (8.5°–20.0°), and e4 ($>$20.0°).

3. Results

3.1. Whole-brain global measures

First, we analyzed the global (across the whole cortical surface) macro- and micro-structure. MRI measures were probed along nine projection levels relative to the white-gray matter boundary ranging from the deep white matter to the pial-gray matter boundary (Fig. 1c). The whole sample was assessed by a linear model, which estimated a Base level, an Age effect, and a CVL group effect (CVL minus NV). At the Base level, the mean cortical thickness (across all vertices sparing the non-cortical medial wall) was 2.63 mm, the mean (white matter) surface area per hemisphere (excluding medial wall) was 817 cm^2, and the mean gray matter volume per hemisphere was 244,486 mm^3. These values were comparable with previous reports (Van Essen and Drury, 1997). All three measures significantly decreased with age (Age effect) at a rate of 0.316% per year [t(70) = 9.1, p < .001] for cortical thickness, 0.198% per year [t(70) = 38.3, p < .001] for surface area, and 0.541% per year [t(70) = 44.7, p < .001] for gray matter volume. Moreover, cortical gyrification as measured by the intrinsic curvature index and folding index (Van Essen and Drury, 1997) increased with age. The intrinsic curvature index increased by 1.638% per year [t(68) = 5.7, p < .001] from a Base level of 243. The folding index increased by 2.659% per year [t(67) = 3.0, p = .004] from a Base level of 1759. No significant group effects (CVL vs. NV) were detectable on these global measures.

Tissue-dependent measures of brain structure (T1w, T2w) varied across projection levels from the deep white matter (2 mm below the white-gray matter boundary) to the pial-gray matter boundary (see Fig. 2). As expected, Base levels of T1w values were relatively high in the white matter and low in the gray matter. T1w values significantly ($p \leq$ .01) decreased along the projection axis (from white to gray matter). However, at the deepest white matter projection a significant increase relative to superficial white matter was observed. An almost opposite pattern across projection levels was observed for T2w values, which were relatively low in white matter and which increased significantly along the projection axis (from white to gray matter) except for the deepest white matter projection (Fig. 2a). For control reasons (see methods) MRI measures were also probed at projections beyond the pial-gray matter boundary in the cerebro-spinal fluid. At these extra-cortical projection levels both tissue-dependent measures showed a significant ($p \leq$ .01) decrease (T1w) and increase (T2w), respectively, relative to gray matter projections. This trend was opposite to that observed in the gray matter suggesting that the maxima (T2w) and minima (T1w) observed in the
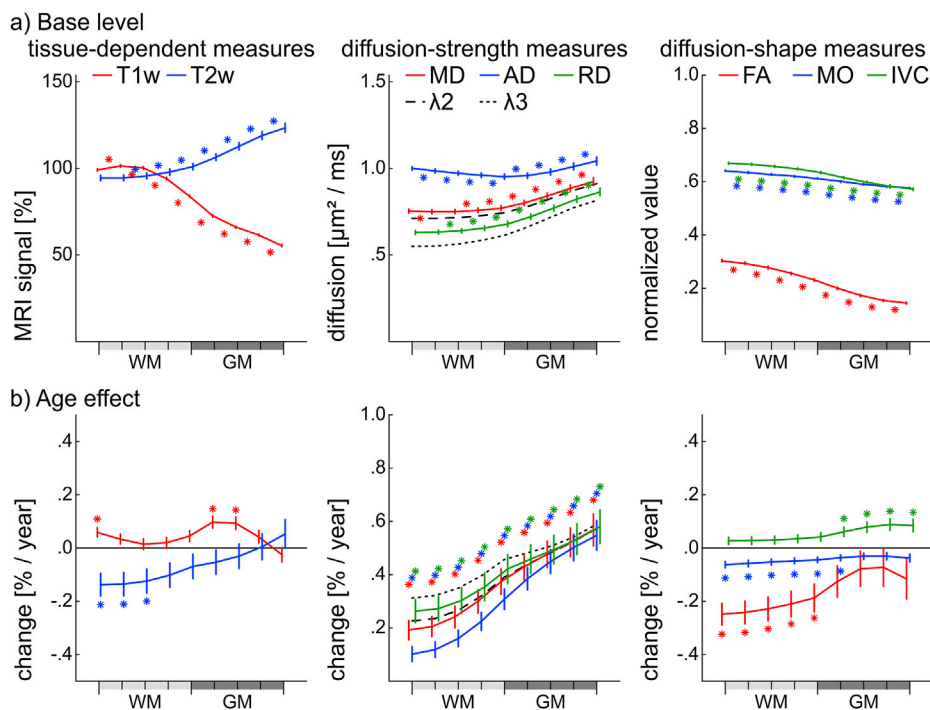
a) Base level

Fig. 2. Summary of global whole-brain measures across projection levels. Projection levels are shown for white (WM) and gray (GM) matter from left to right (2 mm below WGB to PGB). Left column shows tissue-dependent measures (T1w, T2w). Middle column shows measures of diffusion-strength including mean (MD), axial (AD), and radial diffusion (RD). Second and third eigenvalues (λ_2, λ_3) are shown for reference. Right column shows measures of diffusion-shape based on the tensor model: fractional anisotropy (FA), mode of diffusion (MO), and inter-voxel coherence (IVC). Note that MO was linearly rescaled to [0; 1] for display purposes. Further note that acquisition resolution for diffusion-based measures (2.5 mm isotropic) was larger than the distance between projection levels (0.5 mm in WM) effectively resulting in spatial smoothing across levels (see also section 4.3 in text). a) Base level (intercept of regression at age 20 years) separate for each projection level. Stars indicate significant differences ($p \leq .01$) across adjacent projection levels. b) Age effect (slope of regression with age) normalized to the Base level. Stars indicate Age effects significantly ($p \leq .01$) different from zero. Error bars reflect standard error of the mean.

gray matter did not result from volume averaging with bordering cerebro-spinal fluid voxels. Both tissue-dependent measures (T1w, T2w) showed an Age effect (Fig. 2b). Values of T1w significantly increased by about 0.1% per year in the gray matter and values of T2w significantly decreased by more than 0.1% per year at deep white matter projections. No significant Group effect (CVL minus NV) was observed.

Diffusion measures also showed a gradual change across projection levels. Within gray matter, all diffusion-strength measures increased significantly along the projection axis (from white matter surface to pial surface). However, this pattern was different in the white matter: RD (λ_2 and λ_3) remained constant or increased from deep white matter to the white matter surface, but AD (λ_1) decreased along this projection axis resulting in a minimum at the white-gray matter boundary (Fig. 2a, middle column). Measures of diffusion-shape (FA, MO, IVC) showed a significant monotonic decrease along the whole projection axis (from white to gray matter) (Fig. 2a, right column). As expected, fractional anisotropy (FA) was lower in the gray than in the white matter. Moreover, gray matter showed a more planar mode of diffusion (MO) and less inter-voxel coherence (IVC) in the gray compared to the white matter.

All diffusion measures showed an Age effect. This Age effect partially differed for white and gray matter. All diffusion-strength measures significantly increased with age at all projection levels. The increase of MD was about 0.3% per year in white and about 0.5% per year in gray matter (Fig. 2b, middle column). Age also affected measures of diffusion-shape: FA values (>0.2% per year less anisotropy) and MO values (0.03% per year less tubular diffusion) decreased with age in the white matter only. IVC increased with age (0.06% per year more coherence) in the gray matter (Fig. 2b, right column). Again, no significant Group effects (CVL versus NV) were observed.

3.2. Whole-brain factor analysis

The global whole-brain analysis showed age-related changes for all measures of brain structure. In order to test whether these measures are correlated (e.g., reflecting related structural properties) or whether they are independent (e.g., reflecting different structural properties), a principal component factor analysis was performed. This analysis tested all measures for correlations across vertices of the brain surface and

followed the rationale that it should only reveal one or very few components, if diffusion and tissue-dependent measures are highly correlated (and hence redundant), but a relatively large number of components, if the various measures are sensitive to different aspects of the brain structure. Separate PCAs were performed for the Base level, the Age effect, and the Group effect (CVL vs. NV). According to the eigenvalue criterion (see methods) a minimum of 9 components was needed to explain 95% (Base level), 95% (Age effect), and 92% (Group effect) of the variance. Fig. 3 shows the factor loadings (correlation of original variable with component) of the reduced factor space after varimax rotation. As illustrated, diffusion-based and tissue-dependent measures loaded on separate components indicating that there was little correlation between them. Although measures of diffusion-strength (MD, AD, RD) were highly correlated with each other (loading on the same component), they were not correlated with measures of diffusion-shape, tissue-dependent measures, or cortical thickness (loading on different components). Moreover, diffusion-strength in the white matter was associated with a different component than diffusion-strength in the gray matter. Similarly, measures of diffusion-shape (FA, MO, IVC) were associated with distinct components. FA and MO showed selectivity for either gray or white matter, whereas IVC showed no differences across projection levels. Also, tissue-dependent measures (T1w, T2w) loaded on separate components. Cortical thickness (CT) showed only moderate factor loadings suggesting that it is a relatively unspecific measure of brain structure. Communality (proportion of variance explained by the 9 components) was very high (>95%) for most variables except for cortical thickness.

3.3. Whole-brain surface maps

The results of the factor analysis suggest that diffusion-based and tissue-dependent measures are sensitive to distinct components of age-related changes in brain structure. However, it does not reveal the scope of age-related brain changes. This is shown in Fig. 4 separate for each of the tested measures. White and gray matter are plotted separately, but projections within each of these structures were combined as the factor analysis showed distinct components across but not within white and gray matter, respectively. Aging resulted in wide-spread changes of the brain structure. Left and right hemispheres (see also Supp. Figs. S1, S2, S3)
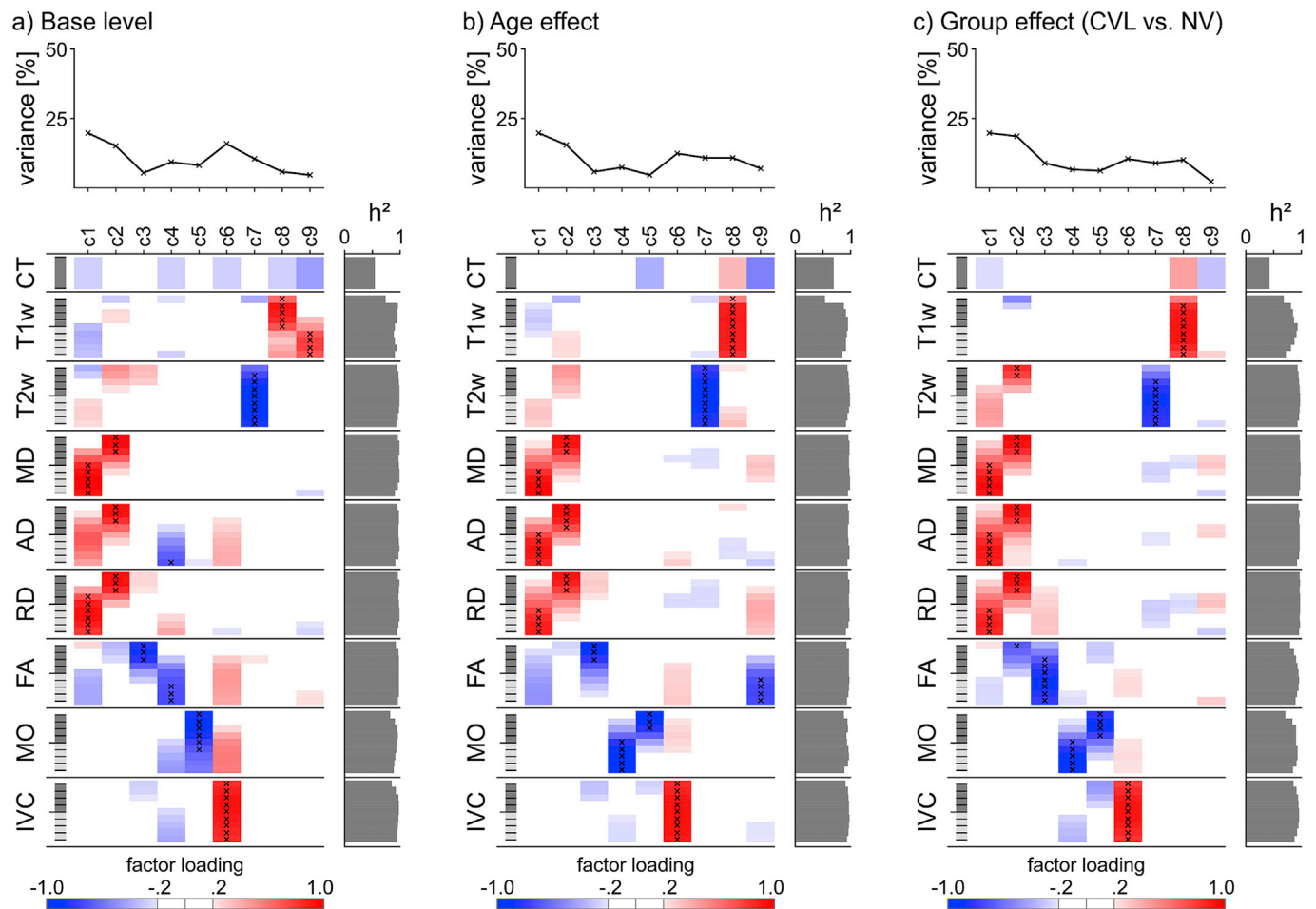
Fig. 3. Results of the factor analysis. Factor loadings (correlations with component) for Base level (a), Age effect (b), and group effect (c) are shown for tissue-dependent measures (T1w, T2w), cortical thickness (CT), measures of diffusion-strength including mean (MD), axial (AD), and radial diffusion (RD), and measures of diffusion-shape including fractional anisotropy (FA), mode of diffusion (MO), and inter-voxel coherence (IVC). All measures (except CT) are shown for all projection levels from white (WM) to gray (GM) matter as indicated by bright (WM) or dark (GM) bars. Note that acquisition resolution for diffusion-based measures (2.5 mm isotropic) was larger than the distance between projection levels (0.5 mm in WM) effectively resulting in spatial smoothing across levels (see also section 4.3 in text). Factor loadings are color-coded (negative in blue, positive in red). Component order was sorted for facilitating comparison. Measures meeting selection criteria (see methods section) were assigned to the component with the highest factor loading as indicated by stars. Right plots show communality (h^2), which indicates for each measure the proportion of explained variance. Top plots show percentage explained variance per component.

showed almost mirror-imaged effects. Cortical thinning (decrease of CT) was observed in the medial occipital cortex (primarily anterior and parieto-occipital parts), precuneus and cingulate cortex (primarily posterior parts), lateral occipital cortex, superior temporal cortex, parietal cortex, the central sulcus (and adjacent pre- and post-central areas), and the insula (primarily posterior parts). Age-related increases in T1w values (both white and gray matter) were primarily observed in the medial frontal cortex (including anterior cingulate cortex and pericallosal sulcus), the frontal pole, the insula (primarily anterior parts), the lateral pre-frontal cortex, and the central sulcus. Age-related decreases in T1w values were limited to small sections of the occipital pole (Supp. Figs. S2 and S3). T2w values decreased by age primarily in the occipital pole and the lateral occipital cortex in both white and gray matter. Additionally, decreased T2w values were observed in the white matter of the anterior cingulate cortex (Supp. Figs. S2 and S3) and increased T2w values were observed in the central sulcus (gray matter only).

The major age-related change in diffusion-based measures was an increase of diffusion-strength, which was more severe and wide-spread for gray than for white matter. Similar brain areas were detected by all measures of diffusion-strength (AD, RD, and MD), but RD and MD seemed to be more sensitive measures than AD for detecting changes in the white matter. Within white matter, an age-related increase in

diffusion was primarily observed in the medial occipital cortex (primarily anterior and parieto-occipital parts), precuneus and cingulate cortex (primarily posterior parts), lateral occipital cortex, temporal cortex, and the insula. Increased diffusion of the gray matter was additionally observed in the medial frontal cortex (including anterior cingulate parts), the frontal pole, the lateral pre-frontal cortex, the central sulcus (and adjacent gyri). Posterior occipital regions and sections of the lateral parietal cortex were relatively spared.

In contrast to the wide-spread effects of diffusion-strength, measures of diffusion-shape showed Age effects only in a few cortical regions. Anisotropy (FA) of the white matter decreased primarily in the medial cortex including the anterior occipital cortex, the parieto-occipital region, the precuneus and parts of the cingulate cortex. The lateral cortex was only affected at sections of the intraparietal sulcus, superior temporal sulcus and the frontal operculum (Supp. Figs. S1, S2, S3). Most of these age-related decreases in FA were only observed in the white but not gray matter. Aging decreased the mode of diffusion (MO) only in a mid-section of the cingulate cortex (gray matter only) and the medial occipital cortex. Inter-voxel coherence (IVC) increased by age primarily in the posterior insula and parts of the temporal cortex (Supp. Figs. S1, S2, S3).

In contrast to the wide-spread Age effects, structural changes related to CVL were more focal: Group effects (CVL vs. NV) were primarily
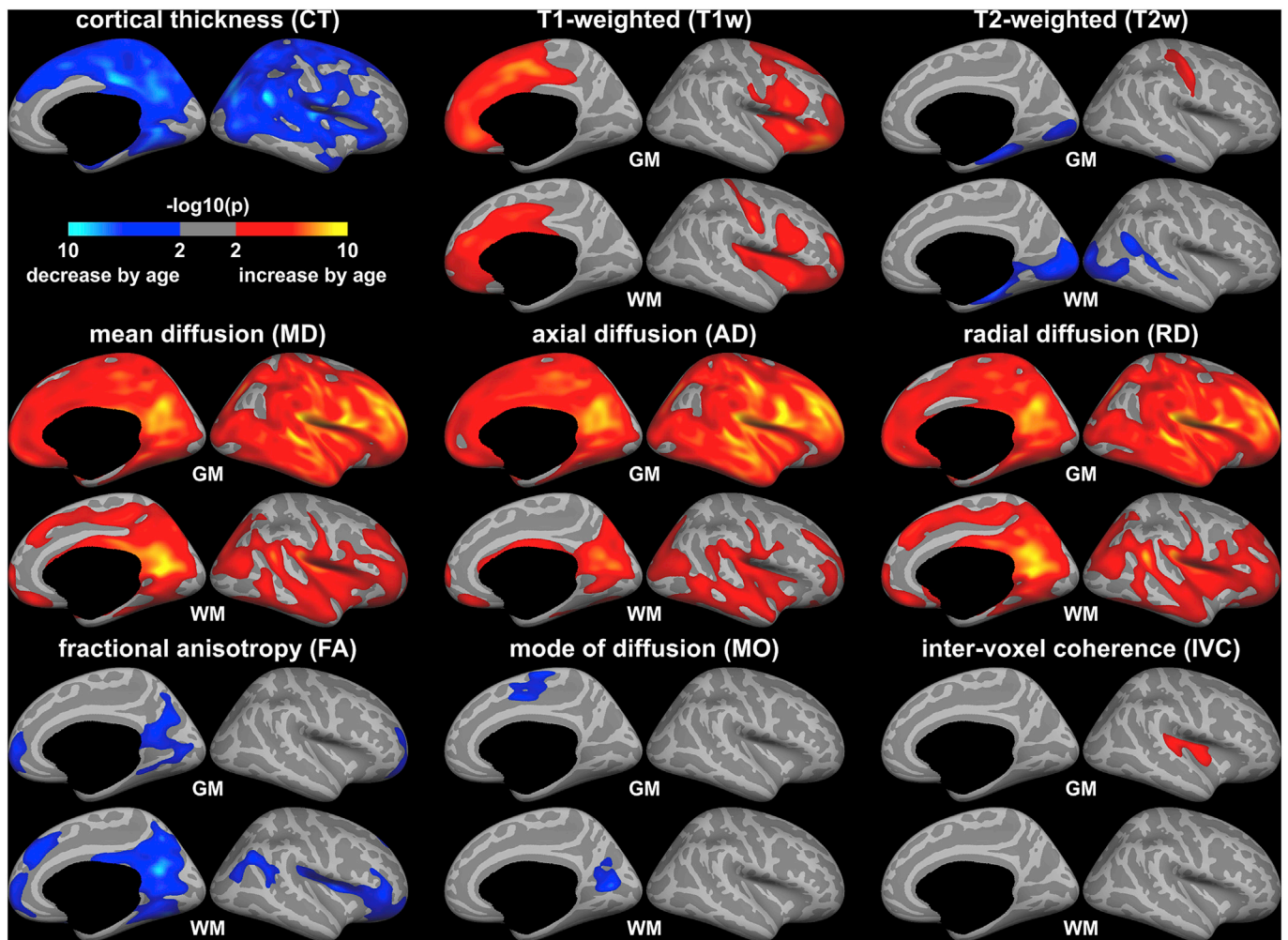
Fig. 4. Surface maps of the Age effect. Significant increases (red/yellow) or decreases (blue) of MR measures by age (slope of regression with age) are overlaid on the right cortical surface (medial and lateral view) of the average brain. Similar results were obtained for the left hemisphere (Supp. Fig. S1) or by analyses including only the normally sighted (NV) group (Supp. Figs. S2 and S3). Top row shows cortical thickness (CT), T1-weighted (T1w), and T2-weighted (T2w) measures. Middle section shows measures of diffusion-strength (MD, AD, RD) and bottom section shows measures of diffusion-shape (FA, MO, IVC). Except for CT all measures are shown separately for projections in white (WM) and gray matter (GM), respectively. Only clusters exceeding a cluster-wise correction for multiple comparisons ($p \leq .01$) are shown.

observed at the occipital pole (Fig. 5) and for measures of cortical thickness and diffusion-strength (MD, AD, RD) primarily in the gray matter. In particular, cortical thinning was found in the CVL group at small sections of the occipital pole and at the posterior cingulate cortex. Differences in T1w or T2w intensities were hardly detected. However, enhanced diffusion (MD, AD, and RD) was observed at the occipital pole (a region representing the central visual field corresponding to the lesion projection zone) and some sections of the lateral occipital cortex in the gray matter of both hemispheres. Anterior medial occipital cortex (corresponding to peripheral visual field representations) and white matter parts were hardly affected. Similarly, hardly any group effects were observed on measures of diffusion-shape (except for FA decreases in the gray matter of the occipital pole).

3.4. ROIs of retinotopic areas

For a more detailed quantification of the brain structure in CVL patients, a ROI analysis of the visual cortex was performed (Fig. 1d). This was motivated by previous findings that reported changes in brain structure (Boucard et al., 2009; Burge et al., 2016; Hernowo et al., 2014; Plank et al., 2011; Prins et al., 2016) and functional activity (Masuda

et al., 2008) specific to parts of the visual cortex that represent the scotoma in the (central) visual field (lesion projection zone). Therefore, the patient (CVL) and control (NV) group was compared in regions of interests (ROIs) representing four eccentricities (e1, e2, e3, e4) of the visual field in V1 and V2. Fig. 6 shows cortical thickness (CT), tissue-dependent measures (T1w, T2w) and diffusion-based measures for each of these ROIs (see Supp. Tables S1, S2, and S3 for detailed values). As with the whole-brain surface maps, projections within (but not across) white and gray matter, respectively, were averaged (see Supp. Fig. S4 for detailed effects per projection level). Irrespective of age and group (Base level), T1w values were similar across all ROIs (Fig. 6a). However, the cortex was thicker in V2 than V1. T2w values were lower in central representations of the visual field (e1) than in more peripheral representations (e2, e3, e4). Values of diffusion-strength (MD, AD, RD) tended to be higher for central (e1, e2) than for peripheral (e3, e4) representations of the visual field and more pronounced diffusion was found in V1 than in V2 and for gray as compared to white matter. Measures of diffusion-shape (MO, IVC) showed fairly uniform values across visual cortex ROIs with the exception of FA, which was relatively low in both white and gray matter, but tended to be higher in central compared to peripheral representations of the V1 and V2 gray matter.
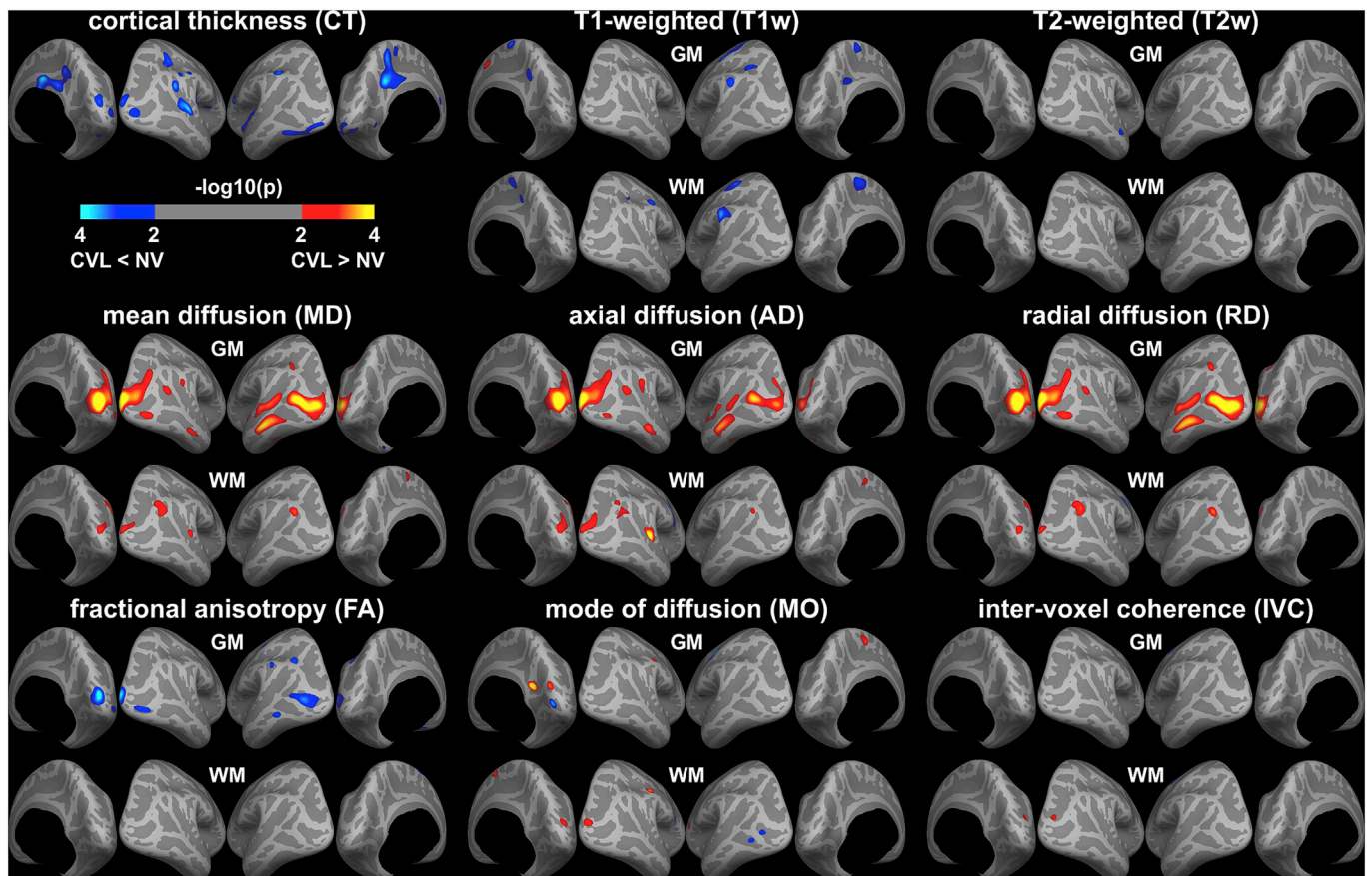
Fig. 5. Surface maps of group effects (CVL vs. NV). Significantly enhanced (red/yellow) or reduced (blue) MR measures for the patient (CVL) compared to the control (NV) group are overlaid on the left and right cortical surfaces of the average brain (lateral and medial views from posterior perspective). Significant differences ($p \leq$ .01, minimum cluster size 50 mm^2) were primarily observed for cortical thickness (CT) and measures of diffusion-strength (MD, AD, RD). Separate maps for projections in white (WM) and gray matter (GM) are shown, respectively.

Almost all measures showed an Age effect (Fig. 6b). This Age effect was comparable for V1 and V2, but differed across eccentricity representations. Age-related cortical thinning (decrease of CT) was observed for peripheral representations (e3, e4) of V1 and V2. By contrast, age-related decreases of T2w (and T1w) values were primarily observed for central representations (e1, e2). Age-related increases of diffusion-strength were primarily observed for peripheral representations of V1 and V2. Similarly, a decrease of FA and MO was observed in peripheral V1 and V2. However, little age-related changes were observed on IVC measures.

Significant differences between CVL patients and the NV control group (Fig. 6c) were primarily observed for cortical thickness (CT) and measures of diffusion-strength (MD, AD, RD). CVL patients compared to controls showed cortical thinning (about 5%) in central visual field representations (e1). Moreover, diffusion-strength (MD, AD, RD) was enhanced by about 5–10% in central visual field representations (e1, e2) of both V1 and V2 (gray matter only). No significant and consistent group differences were observed on measures of diffusion-shape (FA, MO, IVC).

3.5. JMD versus AMD

Our CVL group contained both JMD and AMD patients. The results reported above were based on both sub-groups combined based on the rationale that JMD and AMD patients suffer from similar sensory deprivations (leading to similar secondary degeneration). Nevertheless, it is possible that they differ in the type of structural changes. Therefore, we performed additional analyses separate for the JMD and AMD sub-groups, respectively (Fig. 7, see also Supp. Fig. S5 and Supp. Tables S1,

S2, and S3). Although the main structural changes observed in both sub-groups were cortical thinning and increased diffusion of the occipital pole gray matter, the two sub-groups differed in magnitude and scope. In the JMD group the major structural change was cortical thinning and only a moderate increase in gray matter diffusion limited to the occipital pole and central visual field representations (e1). By contrast, the AMD sub-group showed more wide-spread structural changes: Cortical thinning was not dominant at the occipital pole or central visual ROIs, but instead was primarily observed in the posterior cingulate cortex. However, gray matter diffusion was pronounced in the occipital pole and central visual ROIs (e1, e2). Moreover, increased gray matter diffusion was observed beyond early retinotopic cortex extending to lateral occipital and temporal cortex and the posterior cingulate cortex. The latter effect was also pronounced in direct comparisons of the AMD group with the JMD group (see Supp. Fig. S6).

4. Discussion

We examined the brain macro- and micro-structure of patients with central vision loss and healthy humans in the age range from 19 to 84 years by multimodal MRI including DTI. We found that both, aging and central vision loss, were associated with structural changes in the cortex.

4.1. Degeneration by age

Our results showed that even 'normal' aging is associated with alterations in the cortical brain macro- and micro-structure. We observed age-related reductions in cortical volume and cortical thinning across
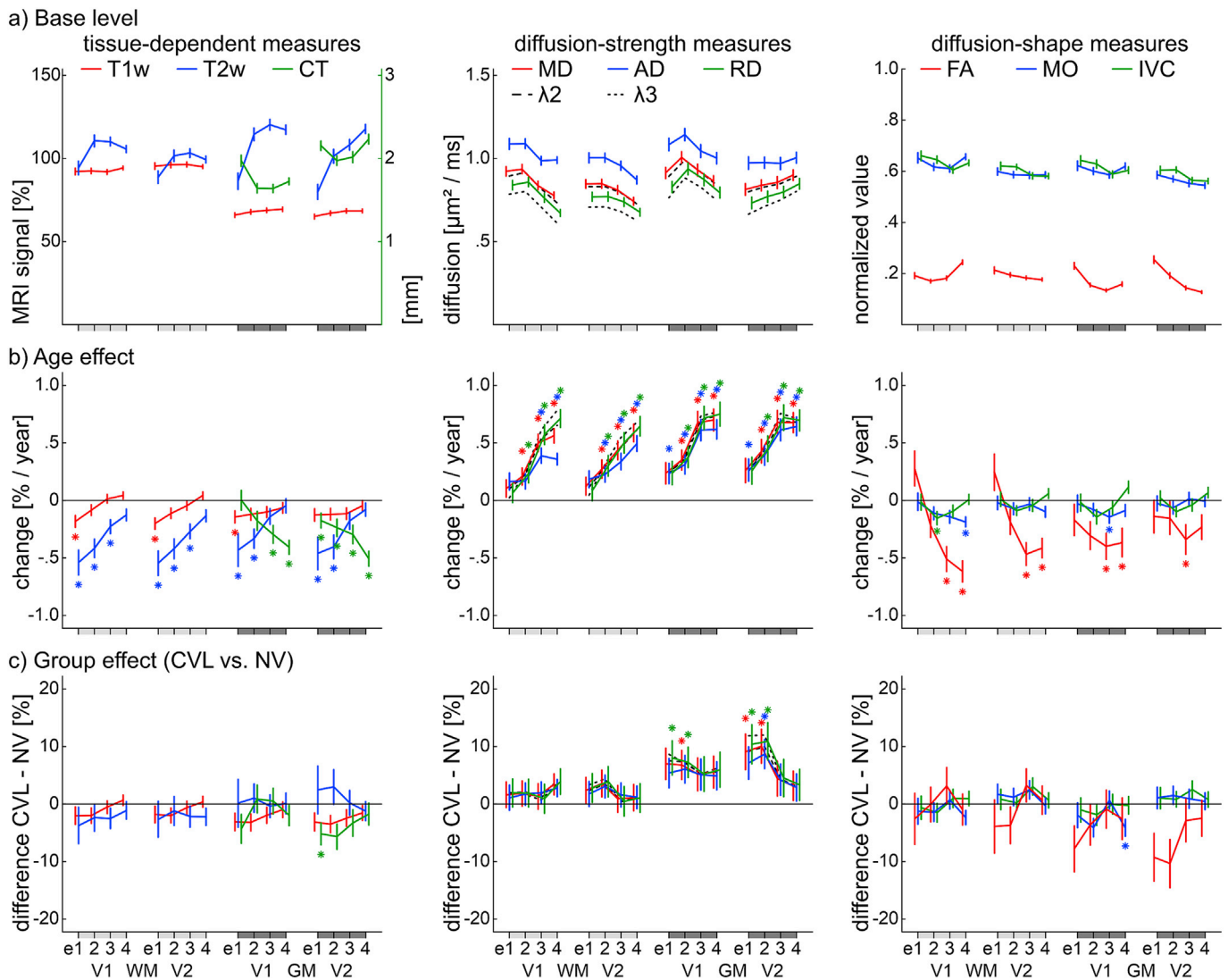
Fig. 6. Means of retinotopic visual cortex ROIs. Left: tissue-dependent measures (T1w, T2w) and cortical thickness (CT). Middle: measures of diffusion-strength including mean (MD), axial (AD), and radial (RD) diffusion and second and third eigenvalues (λ_2, λ_3) for reference. Right: measures of diffusion-shape including fractional anisotropy (FA), mode of diffusion (MO), and inter-voxel coherence (IVC). Primary (V1) and secondary (V2) visual cortex were divided into four eccentricity levels from posterior to anterior (e1, e2, e3, e4) (see also Fig. 1d). Except for CT, white (WM) and gray matter (GM) projections were separated. a) Base level (intercept of regression at age 20 years). b) Age effect (slope of regression with age) normalized to the Base level. c) Group difference (CVL minus NV) normalized to the Base level. Stars (b and c) indicate significant differences from zero ($p \le .01$). Error bars reflect standard error of the mean.

several parts of the cortex. Similar macro-structural changes have been observed in previous studies (Lemaitre et al., 2012; Salat et al., 2004; Sowell et al., 2003; Walhovd et al., 2005). In addition, we observed age-related increases in T1w values in the insula, frontal cortex, and anterior cingulum. Variations in T1w likely reflect myelination (Stüber et al., 2014) or related tissue properties such as extra-cellular water (Gelman et al., 2001), the macromolecular mass fraction (Rooney et al., 2007), and protein and lipid concentrations (Koenig, 1991). Our results further showed age-related decreases in T2w values primarily in the lateral occipital cortex and occipital pole. This finding is consistent with previous work showing faster transverse relaxation in elderly (Korogi et al., 1997). Variations in T2w likely reflect variations in nonheme iron concentrations (Gelman et al., 1999; Korogi et al., 1997) or myelin (Stüber et al., 2014).

Our results further showed pronounced age-related differences in diffusion-based measures. Aging was primarily associated with increased diffusion in both the gray and the superficial white matter. Reduced (less anisotropic) FA, reduced (more planar) MO, and increased (more

coherent) IVC was also observed. These findings seem to be inconsistent with previous research that did not find aging-related changes of diffusion properties in the gray matter (Helenius et al., 2002). Note, however, that a coarser analysis approach (ROI-based, less diffusion directions) was adopted in this previous work. Our results suggest that the micro-structure in the gray and superficial white matter as revealed by DTI is not only affected by brain maturation (<20 years) (Wu et al., 2014), but also by aging (>20 years). Moreover, our findings extend previous reports showing age-related changes of the micro-structure in the white matter (e.g., Burzynska et al., 2010; Camara et al., 2007; Damoiseaux et al., 2009; Pfefferbaum et al., 2000; Sullivan et al., 2010; Zahr et al., 2009).

The observed differences in MRI measures suggest age-related degeneration. Although cortical thinning considered in isolation might be interpreted in alternative ways (e.g., enhanced neural density rather than degeneration), the full pattern suggests the involvement of degenerative mechanisms. For instance, cortical thinning was accompanied by increased diffusion (e.g., MD levels). Increased diffusion likely reflects
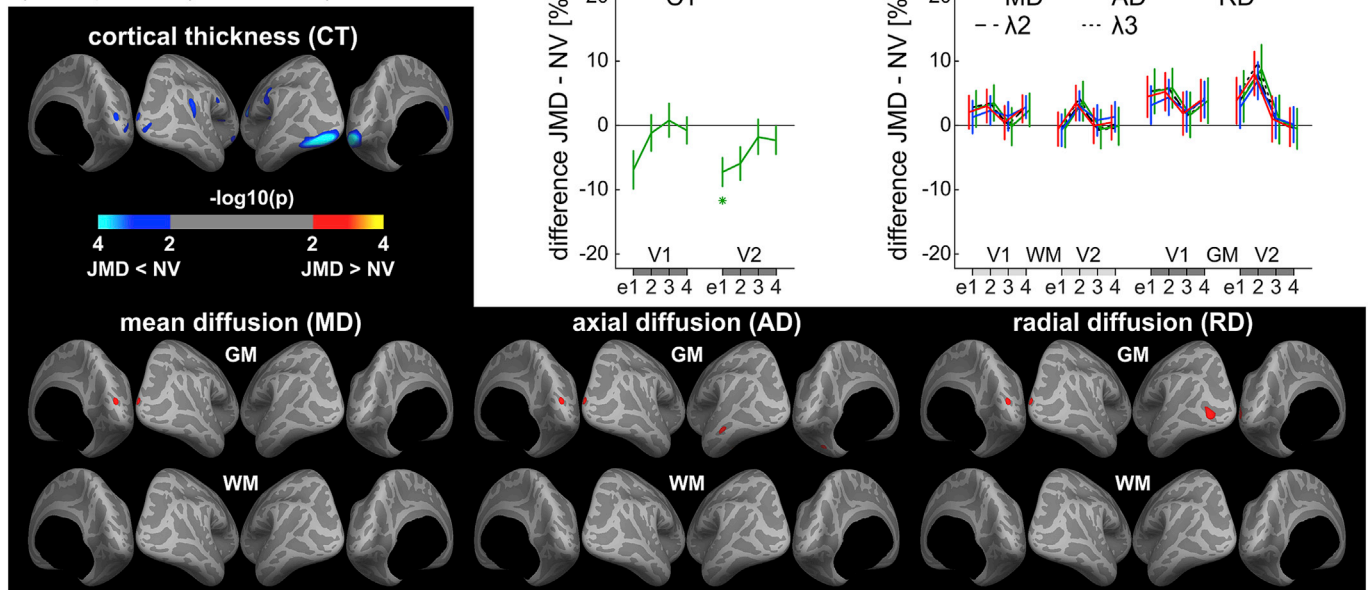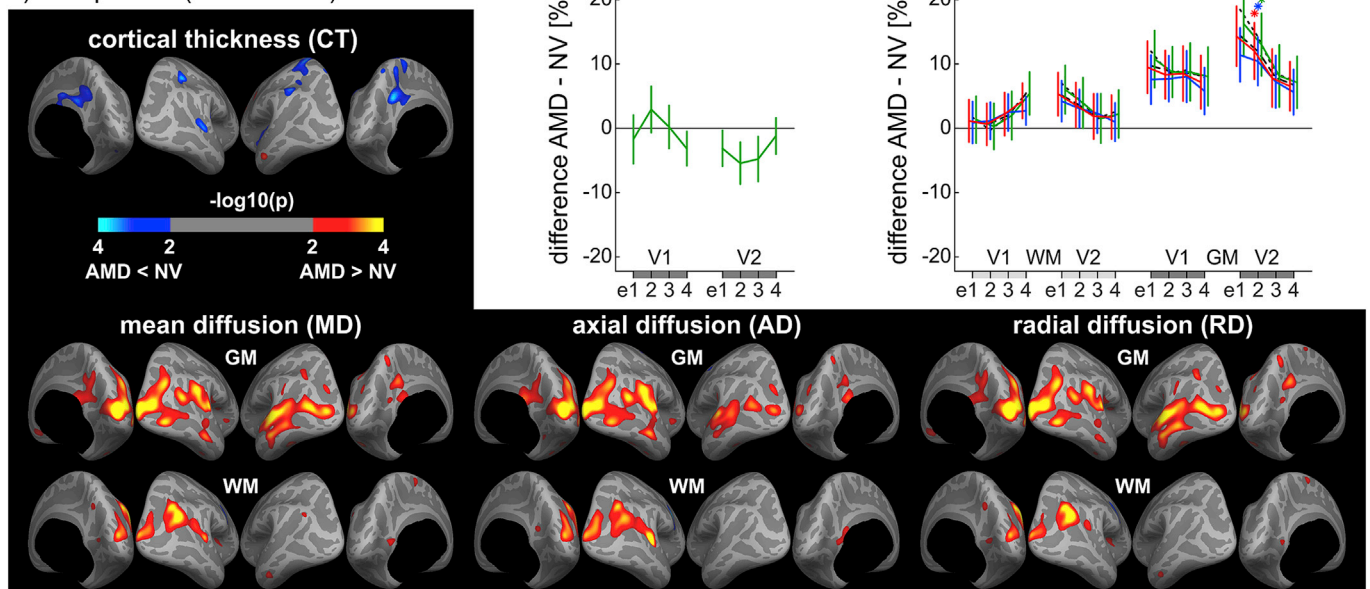
Fig. 7. Group effects separate for JMD and AMD patients. Cortical thickness (CT) and measures of diffusion-strength (MD, AD, RD, and λ_2, λ_3 for reference) are shown separate for the contrast JMD minus NV (a) and AMD minus NV (b). Both surface maps and the means of retinotopic visual cortex ROIs (normalized to Base level) are shown. Significant differences from zero ($p \leq .01$) are indicated color-coded (surface maps) or by stars (ROI means). Error bars in ROI plots reflect standard error of the mean.

cellular lysis (e.g., neural loss) and/or associated gliosis (Govindan et al., 2013; Sotak, 2002; Sykova et al., 1998; Welch et al., 1995). For instance, age-related astrogliosis in rats has been shown to reduce tortuosity (corresponding to increased MD) (Sykova et al., 1998). However, glia proliferation may only account for the Age effects in frontal brain regions that also showed elevated T1w values, because a high macromolecular mass fraction (as to be expected in gliosis) would be associated with fast longitudinal relaxation (corresponding to high T1w values) (Rooney et al., 2007). In other brain regions no differences in T1w were observed. Here, increased diffusion most likely reflects a decline in neural density and/or increase in extracellular space. For instance, increased MD was observed during long-term cell damage (e.g. necrosis) following stroke (Sotak, 2002; Welch et al., 1995) and in brain areas affected by neuronal loss and gliosis such as the seizure-onset regions of epileptic children (Govindan et al., 2013). The occipital pole (including central V1 and V2)

was hardly affected by age-related cortical thinning or alterations in diffusion, but instead by decreased T2w values. These T2w reductions likely reflect a regional-specific increase in nonheme iron deposits (Korogi et al., 1997). Although T2w values are sensitive to both, iron deposits and glia structures such as myelin (Stüber et al., 2014), enhanced myelination (or lipid and protein density) would also decrease diffusion (Sotak, 2002; Xu et al., 2008) and increase T1w values (Koenig, 1991), which was not observed. Iron has only a negligible effect on T1 relaxation (Gelman et al., 2001) or diffusion. The superficial white matter of some cortical areas additionally showed an age-related decline in FA. This decline in anisotropy (FA) may either reflect axonal damage (reduced AD) or impaired membrane integrity and demyelination (enhanced RD) (Xu et al., 2008). Reductions in the mode of diffusion (more planar) may reflect enhanced neurite branching or demyelination. However, enhanced neurite branching and axonal degeneration are

unlikely accounts in those regions affected by FA declines, because no reduction in IVC was observed (Pfefferbaum et al., 2000). Hence, the increased MD and the reduced FA likely reflects de-myelination. We also observed changes in inter-voxel coherence. Originally, this measure was proposed to detect axonal decline in the callosum, which would result in reduced coherence (Pfefferbaum et al., 2000). However, this original work did not observe age-related reductions in inter-voxel coherence, but instead a tendency for increased coherence. Similarly, our results showed that inter-voxel coherence increased by age in some parts of the temporal cortex. Possibly, this increase in coherence reflects reduced axonal complexity (e.g., decline in local association fibers) of the superficial white matter.

Previous studies proposed that age-related degeneration is observed uniformly across the brain (Penke et al., 2010) or in a gradient-like (e.g., anterior to posterior or superior to inferior) manner (Pfefferbaum et al., 2000; Sullivan et al., 2010; Zahr et al., 2009). Our multimodal analysis approach showed that age-related structural changes across the cortex varied by measure and were grouped around several cortical regions. Hence, our findings support a regional-specific view (Burzynska et al., 2010) rather than a global view (at least at the level of the gray and superficial white matter). Our factor analysis (Fig. 3) showed that tissue-dependent and diffusion-based measures were quite independent measures of brain structure suggesting that they are sensitive to distinct age-related mechanisms of degeneration. The surface distribution of cortical thinning and alterations in tissue-dependent measures (T1w or T2w) were hardly related (loading on distinct factors) with age-related changes in DTI metrics. Although measures of diffusion-strength (MD, AD; RD) were highly inter-correlated within gray and white matter, respectively, they were not or only poorly related with measures of diffusion-shape (see factor loadings in Fig. 3). Hence, gradient notions of age-related degeneration are likely constrained to certain brain parts (e.g., deep white matter) and/or are based on unimodal MRI analyses approaches.

4.2. Degeneration following central vision loss

Our results showed that central vision loss due to a macular degeneration resulted in micro-structural changes at a relatively small section of the posterior occipital cortex (V1 and V2) that represents the central visual field (e1, e2) in healthy people and that corresponds to the lesion projection zone in patients. Consistent with previous findings (Burge et al., 2016; Prins et al., 2016), cortical thinning was observed in patients compared to the control group. In addition, the lesion projection zone in V1 and V2 showed enhanced diffusion in the gray matter. Hardly any changes were observed on T1w or T2w values or measures of diffusion-shape (e.g. FA, MO, or IVC). This pattern of structural changes is similar to the age-related changes in other gray matter regions such as the temporal cortex. The enhanced diffusion likely reflects reduced neural density and/or gliosis (Govindan et al., 2013; Sykova et al., 1998). As no or only limited changes in FA were observed, demyelination does not seem to be the major micro-structural change in the lesion projection zone.

CVL did not result in significant changes of diffusion-based or tissue-dependent measures in the superficial white matter. It is possible that the MRI measures were not sensitive enough to detect these group differences or that partial-volume effects obscured them. However, these measures were sensitive in detecting gray matter changes or age-related changes in the superficial white matter of other cortical regions including peripheral representations of V1. Moreover, throughout all comparisons, diffusion-based measures showed less variability and more reliable effects than other measures of brain structure. Hence, CVL-related micro-structural changes in the superficial white matter seem to be either absent or subtler than those observed within the gray matter or those related to aging. It seems that axonal connections (e.g., thalamo-cortical fibers) in the superficial white matter of V1 and V2 were not or only mildly affected by long-lasting sensory deprivation. This is consistent with functional MRI reports that found recovery of visual cortex activity following recovery of retinal function by gene therapy (Ashtari et al., 2011). It must be noted, however, that other studies reported decreased FA values in CVL patients along sections of the subcortical visual pathway such as the optic radiation following central vision loss (Malania et al., 2017; Ogawa et al., 2014; Yoshimine et al., 2018). These micro-structural alterations were primarily observed in sub-cortical structures (e.g., vicinity of the lateral geniculate nucleus).

Our CVL group contained both JMD and AMD patients. Both sub-groups suffered from a damage of foveal and adjacent retinal cells. However, they also differed by several aspects: AMD has a relatively late onset and is caused by the accumulation of drusen that impairs the metabolism of retinal cells (Holz et al., 2004), whereas juvenile macular dystrophy (JMD) subsumes a class of hereditary eye diseases (Boon et al., 2009). Our results showed that in both sub-groups CVL resulted in cortical thinning and increased gray matter diffusion. However, there were also marked differences. Structural changes in JMD patients primarily involved cortical thinning with only a modest increase in GM diffusion suggesting brain atrophy without substantial decline in cellular structures. Moreover, the structural changes were limited to the lesion projection zone of early retinotopic visual areas. By contrast, structural changes in AMD patients were primarily observed in the micro-structure (increased gray matter diffusion). Moreover, structural degeneration was observed beyond early retinotopic visual areas: Enhanced gray matter diffusion was also found in the lateral occipital and temporal cortex. In addition, cortical thinning and increased diffusion was observed in the posterior cingulate cortex. These findings suggest that cortical degeneration in AMD patients is more generalized than in JMD patients.

The structural alterations of AMD patients in lateral brain regions might mediate the reduced functional connectivity of the lateral occipital cortex observed in a previous study (Zhuang et al., 2018). To our knowledge, we are the first to show micro-structural alterations in the lateral cortex of AMD patients. However, altered cytochrome-oxidase staining patterns were observed in area V5 (posterior medial temporal cortex) in a post-mortem examination of an 82-year-old woman (Clarke, 1994). Moreover, reduced gray matter volume of the lateral occipital cortex was observed in patients with monocular blindness (Prins et al., 2017). Note that these wide-spread structural alterations of AMD patients (compared to JMD) are likely not attributable to a more severe visual deprivation. Disease duration and scotoma size tended to be less and visual acuity tended to be higher in AMD than in JMD patients suggesting that low-level visual functions tended to be even less impaired in the AMD than in the JMD sub-group. Hence, the extensive micro-structural alterations in AMD patients are more likely related to higher-level visual functions (e.g., reading) or strategies to compensate for the CVL. Consistent with this notion, reading speed was more strongly compromised in AMD than in JMD patients. It remains elusive though whether these behavioral limitations are the cause or the consequence of the altered brain structure.

It is possible that the AMD-specific alterations in brain structure beyond low-level visual pathways reflect a link between AMD and other neurodegenerative mechanisms such as mild cognitive impairment or Alzheimer's disease (Ikram et al., 2012). According to this view, the pathological mechanisms responsible for the cellular degeneration in the retina of AMD (but not JMD) patients are also operating in the brain. Epidemiological studies showed that age-related macular pathologies are associated with enhanced risks for Alzheimer's disease (Klaver et al., 1999) or cognitive impairments (Pham et al., 2006; Woo et al., 2012). Within this view, it is interesting that we observed cortical thinning (and enhanced diffusion) in the posterior cingulate cortex of AMD patients. Cortical thinning (Lehmann et al., 2010) and reduced metabolism (Minoshima et al., 1997) in the posterior cingulate cortex are characteristic markers for Alzheimer's disease (Leech and Sharp, 2014).

4.3. Methodological considerations

Our surface-based DTI analysis differed from previous volumetric (Burzynska et al., 2010; Camara et al., 2007; Damoiseaux et al., 2009; Draganski et al., 2011) or ROI-based (Malania et al., 2017; Ogawa et al., 2014; Penke et al., 2010; Pfefferbaum et al., 2000; Sullivan et al., 2010; Zahr et al., 2009) approaches. Our approach was motivated by the relevance of the gray and the superficial white matter in brain plasticity. Our findings confirmed that the micro-structure of the superficial white matter differs from the gray matter and the deep white matter (Eastwood and Harrison, 2003; Oishi et al., 2008; Phillips et al., 2016; Suarez-Sola et al., 2009). Diffusion eigenvalues varied across projection levels relative to the white-gray matter boundary. Low diffusion (e.g., MD) and low anisotropy (FA) in gray as compared to white matter was expected based on previous work (Helenius et al., 2002). However, the variation across projection levels was not monotonic (see Fig. 2a). In particular, diffusion of the first eigenvalue (AD) showed an inverted U-shaped distribution suggesting that deep white matter was characterized by other cellular properties than superficial white matter.

The surface-based analysis also mitigated methodological problems of volumetric whole-brain approaches such as inter-subject normalization (Bach et al., 2014). However, it may be argued that partial-volume effects and spatial smoothing across projection levels (0.5 mm in WM) may have compromised our findings as the voxel size (2.5 mm isotropic for diffusion-based measures) was larger than the distance between projection levels. Nevertheless, volume averaging likely had only a negligible effect on our main results: As demonstrated by the factor analysis (Fig. 3), white matter projections were sharply separated from gray matter projections. In order to test whether volume averaging with the cerebro-spinal fluid contaminated our findings, we also examined MRI measures outside the gray matter. This analysis showed that MRI properties differed for projections beyond the pial-gray matter boundary from those observed within the gray matter.

Age effects in our study were only examined by a linear regressor. Previous studies suggested a non-linear (e.g., an inverse U-shaped) relationship (Chang et al., 2015; Yeatman et al., 2014). For instance, MRI correlates increase during childhood and adolescence, peak at around 20–40 years, and decline in elderly. However, these previous studies examined a broader age range (e.g., 7–87 years) and a linear model is likely an acceptable approximation for the age range of the current study (19–84 years). We examined both Age effects and CVL effects in a combined analysis. This allowed us to control for confounding effects of Age on CVL. However, it might be argued that our Age effects were contaminated by CVL effects. Therefore, we performed control analyses including only the normally sighted (NV) group. These analyses (Sup. Figs. S2 and S3) showed very similar result patterns as our main analysis.

Our comparison of diffusion-based measures with tissue-dependent measures revealed several important characteristics. Diffusion-based measures are very sensitive measures. Variability within the same brain tissue (e.g., same projection level of white or gray matter) was quite low. Variability across brains primarily reflected Age and Group effects. Diffusion-based measures were quite specific. Little correlation was found with other measures of brain structure. Cortical thickness showed less specificity than any of the diffusion-based measures. However, a single measure of diffusion (e.g., mean diffusion) is not sufficient to fully explain micro-structural changes due to aging or central vision loss. Although changes in MD were most prominent, some mechanisms were best detected by measures of diffusion-shape.

5. Conclusions

Our surface-based DTI analysis revealed significant age-related changes of the brain micro-structure in the gray and superficial white matter. Aging resulted in cortical thinning, enhanced T1w, reduced T2w, enhanced diffusion, reduced anisotropy, and less tubular diffusion. Structural changes were observed across most of the cortex. However,

DTI-based measures, tissue-dependent measures, and cortical thickness were sensitive to relatively distinct degenerative mechanisms: Whereas frontal regions showed atrophy that is likely accompanied by gliosis, structural changes in occipital brain regions likely reflect reduced neural density, demyelination, and enhanced iron concentrations. Central vision loss resulted in enhanced diffusion in the occipital gray matter (central visual field representation) but preserved integrity of the superficial white matter suggesting that visual deprivation is associated with reduced neural density and gliosis but preserved axonal structures in the lesion projection zone. The micro-structural differences of JMD patients are consistent with secondary degeneration due to sensory deprivation, whereas the micro-structural differences of AMD patients likely result from additional degenerative mechanisms.

Data and code availability statement

All data used for this study are stored at the Institute of Psychology of the University of Regensburg. Data is accessible upon request as far as allowed by guidelines established with the ethics committee of the University of Regensburg. Requests should be addressed to M. W. Greenlee.

Declaration of competing interest

Declarations of interest: none.

CRediT authorship contribution statement

Anton L. Beer: Conceptualization, Methodology, Software, Formal analysis, Writing - original draft, Writing - review & editing, Visualization. **Tina Plank:** Conceptualization, Methodology, Formal analysis, Investigation, Writing - review & editing, Project administration. **Mark W. Greenlee:** Conceptualization, Resources, Writing - review & editing, Supervision, Project administration, Funding acquisition.

Appendix A. Supplementary data

Supplementary data to this article can be found online at https://doi.org/10.1016/j.neuroimage.2020.116670.

References

Gelman, N., Ewing, J.R., Gorell, J.M., Spickler, E.M., Solomon, E.G., 2001. Interregional variation of longitudinal relaxation rates in human brain at 3.0 T: relation to estimated iron and water contents. Magn. Reson. Med. 45 (1), 71–79. https://doi.org/10.1002/1522-2594(200101)45:1<71::aid-mrm1011>3.0.co;2–2.

Pfefferbaum, A., Sullivan, E.V., Hedehus, M., Lim, K.O., Adalsteinsson, E., Moseley, M., 2000. Age-related decline in brain white matter anisotropy measured with spatially corrected echo-planar diffusion tensor imaging. Magn. Reson. Med. 44 (2), 259–268. https://doi.org/10.1002/1522-2594(200008)44:2<259::aid-mrm13>3.0.co;2–6.

Ashtari, M., Cyckowski, L.L., Monroe, J.F., Marshall, K.A., Chung, D.C., Auricchio, A., et al., 2011. The human visual cortex responds to gene therapy-mediated recovery of retinal function. J. Clin. Invest. 121 (6), 2160–2168. https://doi.org/10.1172/JCI57377.

Bach, M., Laun, F.B., Leemans, A., Tax, C.M., Biessels, G.J., Stieltjes, B., et al., 2014. Methodological considerations on tract-based spatial statistics (TBSS). Neuroimage 100, 358–369. https://doi.org/10.1016/j.neuroimage.2014.06.021.

Basser, P.J., Pierpaoli, C., 1996. Microstructural and physiological features of tissues elucidated by quantitative-diffusion-tensor MRI. J. Magn. Reson. B 111 (3), 209–219. https://doi.org/10.1006/jmrb.1996.0086.

Basser, P.J., Mattiello, J., LeBihan, D., 1994. MR diffusion tensor spectroscopy and imaging. Biophys. J. 66 (1), 259–267. https://doi.org/10.1016/S0006-3495(94)80775-1.

Beaulieu, C., 2002. The basis of anisotropic water diffusion in the nervous system - a technical review. NMR Biomed. 15 (7–8), 435–455. https://doi.org/10.1002/nbm.782.

Beer, A.L., Watanabe, T., Ni, R., Sasaki, Y., Andersen, G.J., 2009. 3D surface perception from motion involves a temporal-parietal network. Eur. J. Neurosci. 30 (2–3), 703–713. https://doi.org/10.1111/j.1460-9568.2009.06857.x.

Beer, A.L., Plank, T., Greenlee, M.W., 2011. Diffusion tensor imaging shows white matter tracts between human auditory and visual cortex. Exp. Brain Res. 213 (2–3), 299–308. https://doi.org/10.1007/s00221-011-2715-y.

Benson, N.C., Butt, O.H., Brainard, D.H., Aguirre, G.K., 2014. Correction of distortion in flattened representations of the cortical surface allows prediction of V1-V3 functional organization from anatomy. PLoS Comput. Biol. 10 (3), e1003538 https://doi.org/10.1371/journal.pcbi.1003538.

Boon, C.J., Klevering, B.J., Cremers, F.P., Zonneveld-Vrieling, M.N., Theelen, T., Den Hollander, A.I., et al., 2009. Central areolar choroidal dystrophy. Ophthalmology 116 (4), 771–782. https://doi.org/10.1016/j.ophtha.2008.12.019.

Boucard, C.C., Hernowo, A.T., Maguire, R.P., Jansonius, N.M., Roerdink, J.B., Hooymans, J.M., et al., 2009. Changes in cortical grey matter density associated with long-standing retinal visual field defects. Brain 132 (7), 1898–1906. https://doi.org/10.1093/brain/awp119.

Brown, D.R., 2009. Role of microglia in age-related changes to the nervous system. Sci. World J. 9, 1061–1071. https://doi.org/10.1100/tsw.2009.111.

Burge, W.K., Griffis, J.C., Nenert, R., Elkhetali, A., DeCarlo, D.K., ver Hoef, L.W., et al., 2016. Cortical thickness in human V1 associated with central vision loss. Sci. Rep. 6, 23268. https://doi.org/10.1038/srep23268.

Burzynska, A.Z., Preuschhof, C., Backman, L., Nyberg, L., Li, S.C., Lindenberger, U., et al., 2010. Age-related differences in white matter microstructure: region-specific patterns of diffusivity. Neuroimage 49 (3), 2104–2112. https://doi.org/10.1016/j.neuroimage.2009.09.041.

Camara, E., Bodammer, N., Rodriguez-Fornells, A., Tempelmann, C., 2007. Age-related water diffusion changes in human brain: a voxel-based approach. Neuroimage 34 (4), 1588–1599. https://doi.org/10.1016/j.neuroimage.2006.09.045.

Chang, Y.S., Owen, J.P., Pojman, N.J., Thieu, T., Bukshpun, P., Wakahiro, M.L., et al., 2015. White matter changes of neurite density and fiber orientation dispersion during human brain maturation. PLoS One 10 (6), e0123656. https://doi.org/10.1371/journal.pone.0123656.

Clarke, S., 1994. Modular organization of human extrastriate visual cortex: evidence from cytochrome oxidase pattern in normal and macular degeneration cases. Eur. J. Neurosci. 6 (5), 725–736. https://doi.org/10.1111/j.1460-9568.1994.tb00984.x.

Damoiseaux, J.S., Smith, S.M., Witter, M.P., Sanz-Arigita, E.J., Barkhof, F., Scheltens, P., et al., 2009. White matter tract integrity in aging and Alzheimer's disease. Hum. Brain Mapp. 30 (4), 1051–1059. https://doi.org/10.1002/hbm.20563.

de Brabander, J.M., Kramers, R.J., Uylings, H.B., 1998. Layer-specific dendritic regression of pyramidal cells with ageing in the human prefrontal cortex. Eur. J. Neurosci. 10 (4), 1261–1269. https://doi.org/10.1046/j.1460-9568.1998.00137.x.

Draganski, B., Ashburner, J., Hutton, C., Kherif, F., Frackowiak, R.S., Helms, G., et al., 2011. Regional specificity of MRI contrast parameter changes in normal ageing revealed by voxel-based quantification (VBQ). Neuroimage 55 (4), 1423–1434. https://doi.org/10.1016/j.neuroimage.2011.01.052.

Eastwood, S.L., Harrison, P.J., 2003. Interstitial white matter neurons express less reelin and are abnormally distributed in schizophrenia: towards an integration of molecular and morphologic aspects of the neurodevelopmental hypothesis. Mol. Psychiatr. 8 (9) https://doi.org/10.1038/sj.mp.4001399, 769, 821-731.

Ennis, D.B., Kindlmann, G., 2006. Orthogonal tensor invariants and the analysis of diffusion tensor magnetic resonance images. Magn. Reson. Med. 55 (1), 136–146. https://doi.org/10.1002/mrm.20741.

Fischl, B., 2012. FreeSurfer. Neuroimage 62 (2), 774–781. https://doi.org/10.1016/j.neuroimage.2012.01.021.

Fürntratt, E., 1969. Zur bestimmung der Anzahl interpretierbarer gemeinsamer Faktoren in Faktorenanalysen psychologischer daten. Diagnostica 15, 62–75.

Gelman, N., Gorell, J.M., Barker, P.B., Savage, R.M., Spickler, E.M., Windham, J.P., et al., 1999. MR imaging of human brain at 3.0 T: preliminary report on transverse relaxation rates and relation to estimated iron content. Radiology 210 (3), 759–767. https://doi.org/10.1148/radiology.210.3.r99fe41759.

Govindan, R.M., Asano, E., Juhasz, C., Jeong, J.W., Chugani, H.T., 2013. Surface-based laminar analysis of diffusion abnormalities in cortical and white matter layers in neocortical epilepsy. Epilepsia 54 (4), 667–677. https://doi.org/10.1111/epi.12129.

Grady, C., 2012. The cognitive neuroscience of ageing. Nat. Rev. Neurosci. 13 (7), 491–505. https://doi.org/10.1038/nrn3256.

Hagler Jr., D.J., Saygin, A.P., Sereno, M.I., 2006. Smoothing and cluster thresholding for cortical surface-based group analysis of fMRI data. Neuroimage 33 (4), 1093–1103. https://doi.org/10.1016/j.neuroimage.2006.07.036.

Helenius, J., Soinne, L., Perkio, J., Salonen, O., Kangasmaki, A., Kaste, M., et al., 2002. Diffusion-weighted MR imaging in normal human brains in various age groups. AJNR Am. J. Neuroradiol. 23 (2), 194–199.

Hernowo, A.T., Prins, D., Baseler, H.A., Plank, T., Gouws, A.D., Hooymans, J.M., et al., 2014. Morphometric analyses of the visual pathways in macular degeneration. Cortex 56, 99–110. https://doi.org/10.1016/j.cortex.2013.01.003.

Holz, F.G., Pauleikhoff, D., Klein, R., Bird, A.C., 2004. Pathogenesis of lesions in late age-related macular disease. Am. J. Ophthalmol. 137 (3), 504–510. https://doi.org/10.1016/j.ajo.2003.11.026.

Ikram, M.K., Cheung, C.Y., Wong, T.Y., Chen, C.P., 2012. Retinal pathology as biomarker for cognitive impairment and Alzheimer's disease. J. Neurol. Neurosurg. Psychiatry 83 (9), 917–922. https://doi.org/10.1136/jnnp-2011-301628.

Jolliffe, I.T., 2002. Principal Component Analysis. Springer, New York.

Klaver, C.C., Ott, A., Hofman, A., Assink, J.J., Breteler, M.M., de Jong, P.T., 1999. Is age-related maculopathy associated with Alzheimer's disease? The rotterdam study. Am. J. Epidemiol. 150 (9), 963–968. https://doi.org/10.1093/oxfordjournals.aje.a010105.

Koenig, S.H., 1991. Cholesterol of myelin is the determinant of gray-white contrast in MRI of brain. Magn. Reson. Med. 20 (2), 285–291. https://doi.org/10.1002/mrm.1910200210.

Korogi, Y., Hirai, T., Komohara, Y., Okuda, T., Ikushima, I., Kitajima, M., et al., 1997. T2 shortening in the visual cortex: effect of aging and cerebrovascular disease. AJNR Am. J. Neuroradiol. 18 (4), 711–714.

Leech, R., Sharp, D.J., 2014. The role of the posterior cingulate cortex in cognition and disease. Brain 137 (1), 12–32. https://doi.org/10.1093/brain/awt162.

Lehmann, M., Rohrer, J.D., Clarkson, M.J., Ridgway, G.R., Scahill, R.I., Modat, M., et al., 2010. Reduced cortical thickness in the posterior cingulate gyrus is characteristic of both typical and atypical Alzheimer's disease. J. Alzheimers Dis. 20 (2), 587–598. https://doi.org/10.3233/JAD-2010-1401.

Lemaitre, H., Goldman, A.L., Sambataro, F., Verchinski, B.A., Meyer-Lindenberg, A., Weinberger, D.R., et al., 2012. Normal age-related brain morphometric changes: nonuniformity across cortical thickness, surface area and gray matter volume? Neurobiol. Aging 33 (3). https://doi.org/10.1016/j.neurobiolaging.2010.07.013, 617 e611-619.

Malania, M., Konrad, J., Jagle, H., Werner, J.S., Greenlee, M.W., 2017. Compromised integrity of central visual pathways in patients with macular degeneration. Invest. Ophthalmol. Vis. Sci. 58 (7), 2939–2947. https://doi.org/10.1167/iovs.16-21191.

Masuda, Y., Dumoulin, S.O., Nakadomari, S., Wandell, B.A., 2008. V1 projection zone signals in human macular degeneration depend on task, not stimulus. Cerebr. Cortex 18 (11), 2483–2493. https://doi.org/10.1093/cercor/bhm256.

Minoshima, S., Giordani, B., Berent, S., Frey, K.A., Foster, N.L., Kuhl, D.E., 1997. Metabolic reduction in the posterior cingulate cortex in very early Alzheimer's disease. Ann. Neurol. 42 (1), 85–94. https://doi.org/10.1002/ana.410420114.

Nichols, N.R., Day, J.R., Laping, N.J., Johnson, S.A., Finch, C.E., 1993. GFAP mRNA increases with age in rat and human brain. Neurobiol. Aging 14 (5), 421–429. https://doi.org/10.1016/0197-4580(93)90100-p.

Ogawa, S., Takemura, H., Horiguchi, H., Terao, M., Haji, T., Pestilli, F., et al., 2014. White matter consequences of retinal receptor and ganglion cell damage. Invest. Ophthalmol. Vis. Sci. 55 (10), 6976–6986. https://doi.org/10.1167/iovs.14-14737.

Oishi, K., Zilles, K., Amunts, K., Faria, A., Jiang, H., Li, X., et al., 2008. Human brain white matter atlas: identification and assignment of common anatomical structures in superficial white matter. Neuroimage 43 (3), 447–457. https://doi.org/10.1016/j.neuroimage.2008.07.009.

Pakkenberg, B., Pelvig, D., Marner, L., Bundgaard, M.J., Gundersen, H.J., Nyengaard, J.R., et al., 2003. Aging and the human neocortex. Exp. Gerontol 38 (1–2), 95–99. https://doi.org/10.1016/s0531-5565(02)00151-1.

Penke, L., Munoz Maniega, S., Murray, C., Gow, A.J., Hernandez, M.C., Clayden, J.D., et al., 2010. A general factor of brain white matter integrity predicts information processing speed in healthy older people. J. Neurosci. 30 (22), 7569–7574. https://doi.org/10.1523/JNEUROSCI.1553-10.2010.

Peters, A., 2009. The effects of normal aging on myelinated nerve fibers in monkey central nervous system. Front. Neuroanat. 3, 11. https://doi.org/10.3389/neuro.05.011.2009.

Peters, A., Sethares, C., Luebke, J.I., 2008. Synapses are lost during aging in the primate prefrontal cortex. Neuroscience 152 (4), 970–981. https://doi.org/10.1016/j.neuroscience.2007.07.014.

Pham, T.Q., Kifley, A., Mitchell, P., Wang, J.J., 2006. Relation of age-related macular degeneration and cognitive impairment in an older population. Gerontology 52 (6), 353–358. https://doi.org/10.1159/000094984.

Phillips, O.R., Joshi, S.H., Piras, F., Orfei, M.D., Iorio, M., Narr, K.L., et al., 2016. The superficial white matter in Alzheimer's disease. Hum. Brain Mapp. 37 (4), 1321–1334. https://doi.org/10.1002/hbm.23105.

Plank, T., Frolo, J., Brandl-Ruhle, S., Renner, A.B., Hufendiek, K., Helbig, H., et al., 2011. Gray matter alterations in visual cortex of patients with loss of central vision due to hereditary retinal dystrophies. Neuroimage 56 (3), 1556–1565. https://doi.org/10.1016/j.neuroimage.2011.02.055.

Plank, T., Frolo, J., Farzana, F., Brandl-Ruhle, S., Renner, A.B., Greenlee, M.W., 2013. Neural correlates of visual search in patients with hereditary retinal dystrophies. Hum. Brain Mapp. 34 (10), 2607–2623. https://doi.org/10.1002/hbm.22088.

Plank, T., Frolo, J., Brandl-Ruhle, S., Renner, A.B., Jagle, H., Greenlee, M.W., 2017. fMRI with central vision loss: effects of fixation locus and stimulus type. Optom. Vis. Sci. 94 (3), 297–310. https://doi.org/10.1097/OPX.0000000000001047.

Prins, D., Plank, T., Baseler, H.A., Gouws, A.D., Beer, A., Morland, A.B., et al., 2016. Surface-based analyses of anatomical properties of the visual cortex in macular degeneration. PloS One 11 (1), e0146684. https://doi.org/10.1371/journal.pone.0146684.

Prins, D., Jansonius, N.M., Cornelissen, F.W., 2017. Loss of binocular vision in monocularly blind patients causes selective degeneration of the superior lateral occipital cortices. Invest. Ophthalmol. Vis. Sci. 58 (2), 1304–1313. https://doi.org/10.1167/iovs.16-20404.

Resnikoff, S., Pascolini, D., Etya'ale, D., Kocur, I., Pararajasegaram, R., Pokharel, G.P., et al., 2004. Global data on visual impairment in the year 2002. Bull. World Health Organ. 82 (11), 844–851.

Rooney, W.D., Johnson, G., Li, X., Cohen, E.R., Kim, S.G., Ugurbil, K., et al., 2007. Magnetic field and tissue dependencies of human brain longitudinal 1H2O relaxation in vivo. Magn. Reson. Med. 57 (2), 308–318. https://doi.org/10.1002/mrm.21122.

Rosengarth, K., Keck, I., Brandl-Ruhle, S., Frolo, J., Hufendiek, K., Greenlee, M.W., et al., 2013. Functional and structural brain modifications induced by oculomotor training in patients with age-related macular degeneration. Front. Psychol. 4, 428. https://doi.org/10.3389/fpsyg.2013.00428.

Salat, D.H., Buckner, R.L., Snyder, A.Z., Greve, D.N., Desikan, R.S., Busa, E., et al., 2004. Thinning of the cerebral cortex in aging. Cerebr. Cortex 14 (7), 721–730. https://doi.org/10.1093/cercor/bhh032.

Sotak, C.H., 2002. The role of diffusion tensor imaging in the evaluation of ischemic brain injury - a review. NMR Biomed. 15 (7–8), 561–569. https://doi.org/10.1002/nbm.786.

Sowell, E.R., Peterson, B.S., Thompson, P.M., Welcome, S.E., Henkenius, A.L., Toga, A.W., 2003. Mapping cortical change across the human life span. Nat. Neurosci. 6 (3), 309–315. https://doi.org/10.1038/nn1008.

Stevens, J., 2002. Applied Multivariate Statistics for the Social Sciences. Erlbaum, Mahwah, NJ.

Stüber, C., Morawski, M., Schäfer, A., Labadie, C., Wähnert, M., Leuze, C., et al., 2014. Myelin and iron concentration in the human brain: a quantitative study of MRI contrast. Neuroimage 93 (Pt 1), 95–106. https://doi.org/10.1016/j.neuroimage.2014.02.026.

Suarez-Sola, M.L., Gonzalez-Delgado, F.J., Pueyo-Morlans, M., Medina-Bolivar, O.C., Hernandez-Acosta, N.C., Gonzalez-Gomez, M., et al., 2009. Neurons in the white matter of the adult human neocortex. Front. Neuroanat. 3, 7. https://doi.org/10.3389/neuro.05.007.2009.

Sullivan, E.V., Rohlfing, T., Pfefferbaum, A., 2010. Quantitative fiber tracking of lateral and interhemispheric white matter systems in normal aging: relations to timed performance. Neurobiol. Aging 31 (3), 464–481. https://doi.org/10.1016/j.neurobiolaging.2008.04.007.

Sykova, E., Mazel, T., Simonova, Z., 1998. Diffusion constraints and neuron-glia interaction during aging. Exp. Gerontol. 33 (7–8), 837–851. https://doi.org/10.1016/s0531-5565(98)00038-2.

Tang, Y., Nyengaard, J.R., Pakkenberg, B., Gundersen, H.J., 1997. Age-induced white matter changes in the human brain: a stereological investigation. Neurobiol. Aging 18 (6), 609–615. https://doi.org/10.1016/s0197-4580(97)00155-3.

Van Essen, D.C., Drury, H.A., 1997. Structural and functional analyses of human cerebral cortex using a surface-based atlas. J. Neurosci. 17 (18), 7079–7102. https://doi.org/10.1523/JNEUROSCI.17-18-07079.1997.

Walhovd, K.B., Fjell, A.M., Reinvang, I., Lundervold, A., Dale, A.M., Eilertsen, D.E., et al., 2005. Effects of age on volumes of cortex, white matter and subcortical structures. Neurobiol. Aging 26 (9), 1261–1270. https://doi.org/10.1016/j.neurobiolaging.2005.05.020.

Welch, K.M., Windham, J., Knight, R.A., Nagesh, V., Hugg, J.W., Jacobs, M., et al., 1995. A model to predict the histopathology of human stroke using diffusion and T2-weighted magnetic resonance imaging. Stroke 26 (11), 1983–1989. https://doi.org/10.1161/01.str.26.11.1983.

Woo, S.J., Park, K.H., Ahn, J., Choe, J.Y., Jeong, H., Han, J.W., et al., 2012. Cognitive impairment in age-related macular degeneration and geographic atrophy. Ophthalmology 119 (10), 2094–2101. https://doi.org/10.1016/j.ophtha.2012.04.026.

Woolrich, M.W., Jbabdi, S., Patenaude, B., Chappell, M., Makni, S., Behrens, T., et al., 2009. Bayesian analysis of neuroimaging data in FSL. Neuroimage 45 (1 Suppl. l), S173–S186. https://doi.org/10.1016/j.neuroimage.2008.10.055.

Wu, M., Lu, L.H., Lowes, A., Yang, S., Passarotti, A.M., Zhou, X.J., et al., 2014. Development of superficial white matter and its structural interplay with cortical gray matter in children and adolescents. Hum. Brain Mapp. 35 (6), 2806–2816. https://doi.org/10.1002/hbm.22368.

Xu, J., Sun, S.W., Naismith, R.T., Snyder, A.Z., Cross, A.H., Song, S.K., 2008. Assessing optic nerve pathology with diffusion MRI: from mouse to human. NMR Biomed. 21 (9), 928–940. https://doi.org/10.1002/nbm.1307.

Yeatman, J.D., Wandell, B.A., Mezer, A.A., 2014. Lifespan maturation and degeneration of human brain white matter. Nat. Commun. 5, 4932. https://doi.org/10.1038/ncomms5932.

Yoshimine, S., Ogawa, S., Horiguchi, H., Terao, M., Miyazaki, A., Matsumoto, K., et al., 2018. Age-related macular degeneration affects the optic radiation white matter projecting to locations of retinal damage. Brain Struct. Funct. 223 (8), 3889–3900. https://doi.org/10.1007/s00429-018-1702-5.

Zahr, N.M., Rohlfing, T., Pfefferbaum, A., Sullivan, E.V., 2009. Problem solving, working memory, and motor correlates of association and commissural fiber bundles in normal aging: a quantitative fiber tracking study. Neuroimage 44 (3), 1050–1062. https://doi.org/10.1016/j.neuroimage.2008.09.046.

Zecca, L., Youdim, M.B., Riederer, P., Connor, J.R., Crichton, R.R., 2004. Iron, brain ageing and neurodegenerative disorders. Nat. Rev. Neurosci. 5 (11), 863–873. https://doi.org/10.1038/nrn1537.

Zheng, W., Chee, M.W., Zagorodnov, V., 2009. Improvement of brain segmentation accuracy by optimizing non-uniformity correction using N3. Neuroimage 48, 73–83. https://doi.org/10.1016/j.neuroimage.2009.06.039.

Zhuang, J., Madden, D.J., Duong-Fernandez, X., Chen, N.K., Cousins, S.W., Potter, G.G., et al., 2018. Language processing in age-related macular degeneration associated with unique functional connectivity signatures in the right hemisphere. Neurobiol. Aging 63, 65–74. https://doi.org/10.1016/j.neurobiolaging.2017.11.003.